Supporting Material to:

Title: What Are the Oxidation States of Manganese Required to Catalyze Photosynthetic Water Oxidation?

Authors: [†, ¶]Derrick R. J. Kolling, [‡, ‖]Nicholas Cox, [§]Gennady M. Ananyev, [‡]Ron J. Pace, and [§]G. Charles Dismukes*

Affiliations: [†]Department of Chemistry, Princeton University, Princeton, NJ 08544; [‡]Research School of Chemistry, Australian National University, Canberra, ACT 0200, Australia; [§]Department of Chemistry & Chemical Biology, Waksman Institute, Rutgers University, Piscataway, NJ 08854

***Corresponding author:** Email address: dismukes@rci.rutgers.edu

Current Address: [¶]Department of Chemistry, Marshall University, One John Marshall Drive, Huntington, WV 25755; [‖]Max-Planck-Institut für Bioanorganische Chemie, Stiftstrasse 34-36, D-45470 Mülheim an der Ruhr, Germany.

Table S1: Kok parameters for intact and re-assembled PS II membranes in the presence of 2 mM ferricyanide

	Intact (short incubation in $FeCN_6$)	Intact (long incubation in $FeCN_6$)	Reassembled
α	16%	16%[b]	34%
γ	75%	75%[b]	56%
β	9%	9%[b]	9%[b]
ε	0.02%	0.02%[b]	0.02%[b]
S_0 (Q_AFe^{2+})	43%	46%	49%
S_1 (Q_AFe^{2+})	57%	37%	38%
S_1 (Q_AFe^{3+})	0%	17%	13%

[b]Fixed parameters.

Table S2: Kok parameters (as % of 100) for photo-assembly models IM2, IM4 and IM4 (constrained).

	IM2	IM4[a]	IM4 (constrained)
α_1	~20	~87	0
α_2	~70	~0	0
α_3	-	~0	0
α_4	-	~66	0
IM_1*	100[b]	31	100[b]
IM_2	0[b]	21	0[b]
IM_3	-	25	0[b]
IM_4	-	23	0[b]

[b]Fixed parameters. [a]Non-unique solution. Kok parameters for S-state transitions are assumed to be the same as for re-assembled PS II (see table 1, column 3). Pre-oxidized non-heme-iron was assumed to be 10%.

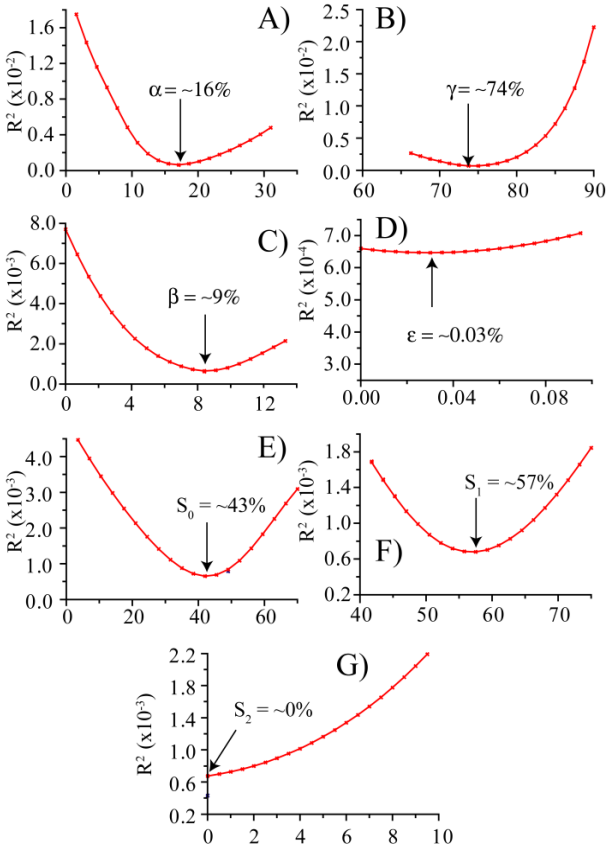

Figure S1: Graphical analysis of the solution space of the fitting to the O_2 oscillation pattern in intact PS II membranes (Fig. 2A) to assess the uniqueness of the solutions. Individual tiles (A-G) represent the one co-ordinate residue (R^2) landscape of each Kok parameter. Each point (marked with a cross) in the plots represents an optimized non-linear least squares fitting, while the combination of red lines and crosses represent the solution space generated by using the simple Kok model (40). Populations of the initial (dark adapted) S-states are given for S_0, S_1 and S_2.

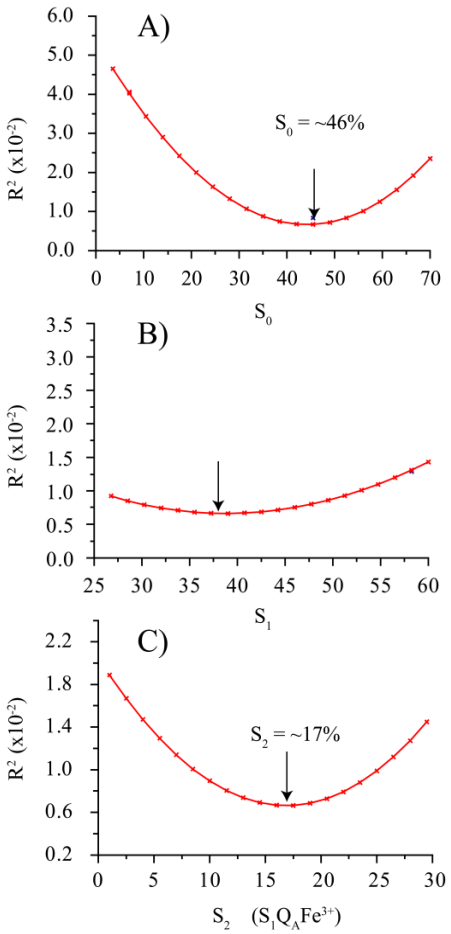

Figure S2: Graphical analysis of the solution space of the fitting to the O_2 oscillation pattern in intact PS II membranes (Fig. 2B). Individual tiles (A-C) represent the one co-ordinate residue (R^2) landscape of Kok parameter: S_0, S_1 and S_2. Each point (marked with a cross) represents an optimized non-linear least squares fitting. Red lines/crosses: solution space using the simple Kok model (40). As stated in the main text, the 'dark adaptation' time used to synchronize the S-states can alter the observed O_2 oscillation pattern. Long incubations in $Fe(CN)_6$ result in a more rapid dampening of oscillations and a noticeable increase in the O_2 yield on the 2nd flash (29,36). This effect occurs because the $Fe(CN)_6$ added to the sample for the purpose of extracting electrons from PS II via Q_B (the mobile electron acceptor), will partially oxidize the non-heme iron in the dark. The non-heme iron of PS II (Fe^{2+}, midpoint potential 470 mV at pH 5.9) can act as an addition electron acceptor for the enzyme if oxidized (Fe^{3+}) and reduction of the oxidized non-heme iron by $P680^*$ (via Q_A^-) occurs very quickly in comparison to reduction of Q_B. As a result, a 60 us flash is sufficient to reduce both the non-heme iron and the Q_B, which results in a double hit. The fitting of the O_2 oscillation pattern in Fig. 3B was re-optimized to include this effect. Here it was assumed that the flash response (α, γ, β, ε) of the 'long incubation' sample was identical to the 'short incubation' sample and the initial S-state populations (S_0, S_1 and S_2) were allowed to change. An S_2 population is nominally equivalent to the $S_1Q_AFe^{3+}$ state. As above, the solution space for this fitting was examined and can be seen in Tiles E, F, and G. The solution yielded a significantly larger S_2 ($S_1Q_AFe^{3+}$) population (17-18%) when compared to the 'short incubation' fitting (0-5%), as would be expected if the non-heme iron were oxidized by

ferricyanide, the electron acceptor. The latter was confirmed by EPR spectroscopy, which showed that longer incubation times led to the generation of oxidized Fe^{3+} (Fig. S4).

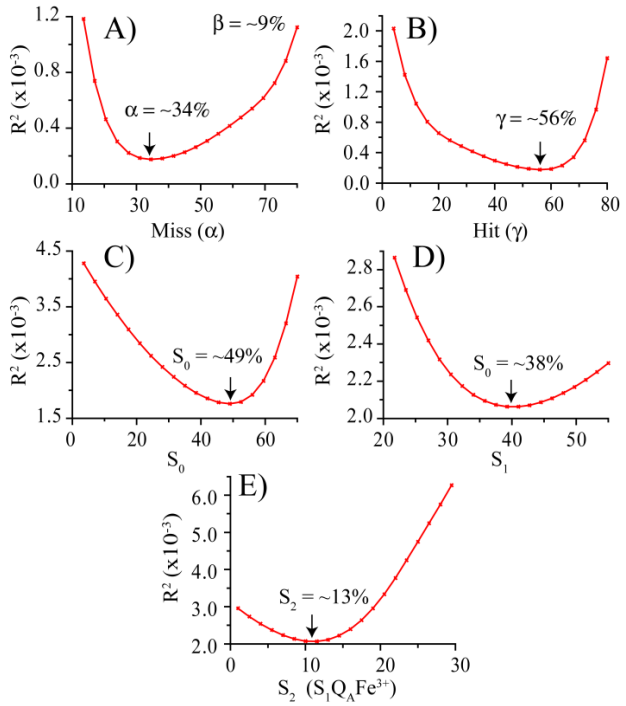

Figure S3: Graphical analysis of the solution space of the fitting to the O_2 oscillation pattern in reassembled apo-WOC membranes (Fig. 2C). Individual tiles (A-E) represent the one co-ordinate residue (R^2) landscape of Kok parameter: α, γ, β, ε, S_0, S_1 and S_2. Each point (marked with a cross) represents an optimized non-linear least squares fitting. Red lines/crosses: solution space using the simple Kok model (40). As stated in the main text, there is no unique fitting of the O_2 pattern observed in reassembled apo-WOC using the Kok models discussed above. This originates from three previously established observations; 1) reconstituted centers operate in the absence of the three extrinsic protein subunits which provide a substantially higher probability for S-state advance (54,56,57), 2) these subunits also protect the OEC from external reductants that short-circuit S-state cycling, and 3) the presence of excess Mn^{2+} in the photo-assembly buffer is required for high efficiency in photo-assembly but also introduces sacrificial electron donors (free Mn^{2+}aquo and Mn^{2+}bicarbonate) which compete with the native (photo-assembly) sites (37,58). Therefore, to obtain a constrained fitting, the number of free parameters was decreased. Two parameters were fixed in these simulations: double turnovers (β) and inactivation (ε). These two parameters were chosen for the following reasons: 1) The double hit parameter must be less than or equal to that for intact PS II centers (maximum of 9%) since the quantum efficiency is reduced. For spinach PSII centers, the rate limiting step for S-state advancement is the electron transfer step from Q_A to Q_B. The functionality and or size of the acceptor side PQ pool decreases during the procedure for removal of the Mn cluster, leading to a larger miss (and smaller double hit) parameter. Hence, the double hit parameter (β) was set to

9% (the same as intact PS II). 2) The inactivation parameter is insignificant when using red light and short pulses as used here (35,36). Hence the inactivation parameter (ε) was set to 0.02% (the same as intact PS II).
As with the O_2 oscillation pattern from intact PS II, the solution space for fitting the O_2 oscillation pattern of reassembled centers was examined. The one-co-ordinate residue (R^2) landscapes of the Kok parameters α, γ, S_0, S_1 and S_2 are given in Fig. S3. The residues (R^2) values derived from this fitting are significantly larger than that observed for the intact sample (scaled to the absolute intensity). Similarly, all parameters are less well defined. As expected, reassembled PS II have a significantly larger miss value and a non-trivial dark S_2 ($S_1Q_AFe^{3+}$) population (for the reasons discussed in the main text).

Non-heme iron oxidation. Extending the time of dark incubation of the PSII-enriched membranes in the presence of ferricyanide changes the observed O_2 oscillation pattern in a systematic way. Longer incubation results in a more rapid dampening of oscillations, and a noticeable increase in the O_2 yield on the 2^{nd} flash (28, 36). This previously observed phenomenon occurs because ferricyanide slowly oxidizes the non-heme iron (normally ferrous) of the iron-plastoquinone acceptor, which then acts as an additional one-electron acceptor for PSII (47). As a result, the 60 μs flash used here is sufficient to reduce both the oxidized non-heme iron and Q_B, resulting in a double hit on the first flash of the pulse train. This conclusion was confirmed four ways: 1) the dependence of flash O_2 yield on ferricyanide concentration and dark incubation time, 2) the dependence of the 2^{nd}-flash O_2 yield on the flash duration (Fig. 3), 3) EPR spectroscopic measurements of the yield of oxidized non-heme iron in more concentrated samples (Fig. S4) (47), and 4) the EPR kinetics of its oxidation by ferricyanide.

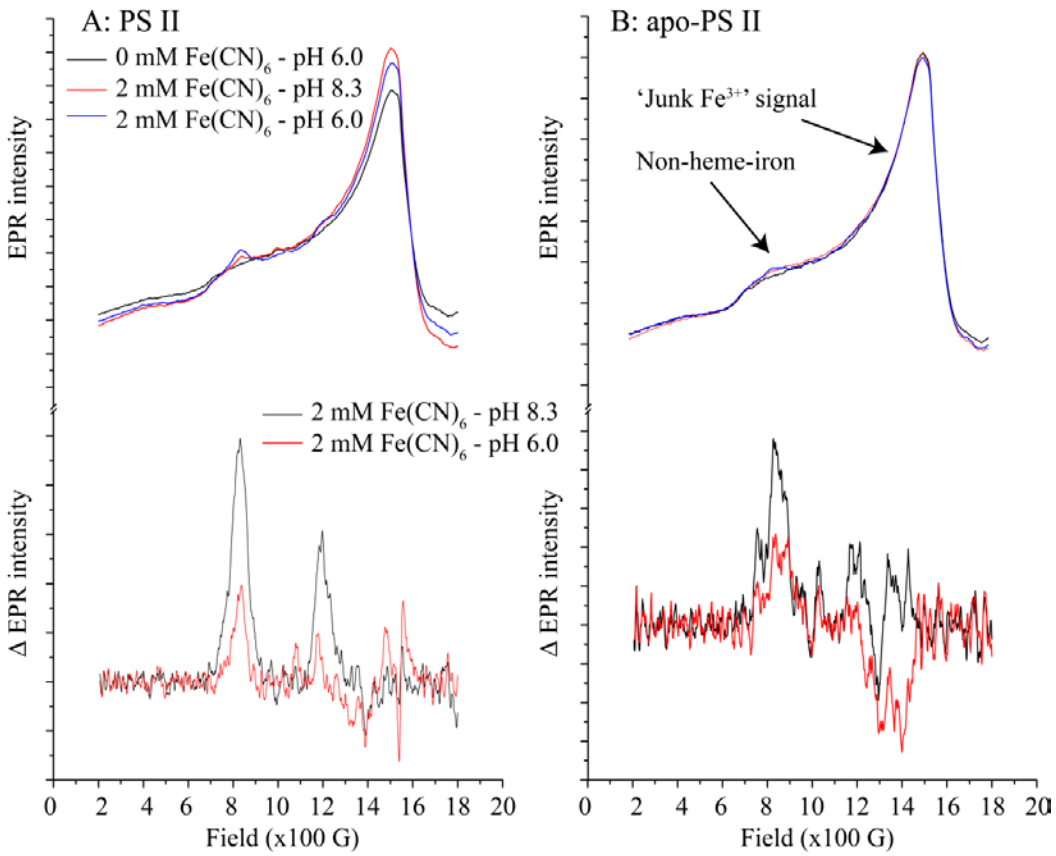

Figure S4: CW X-band EPR controls for the non-heme-iron of PS II. Tile A: Intact PS II subjected to 0 or 2 mM $K_3Fe(CN)_6$ and pH 6.0 or 8.3. Tile B: Apo-WOC. The extent of oxidation of the non-heme-iron in the presence of $Fe(CN)_6$ was independently determined using CW X-band EPR The oxidized non-heme-iron (Fe^{3+}, S = 5/2 ground state) has a broad structured signal that is easily identified. Its most readily observed turning points are seen at g~5.6 and g~8.5 (59, 60). To estimate the initial amount of oxidized non-heme-iron signal, PS II samples were measured under standard photo-assembly conditions (pH 6.0, 2 mM $Fe(CN)_6$) and under conditions where the non-heme-iron is expected to be fully oxidized (pH 8.3, 2 mM $Fe(CN)_6$) (59,60). It was determined that potentially 30% of centers had an oxidized non-heme iron after long dark adaptation (>20 min, see Fig S3 Tile B). This artifact is taken into account in the simulations above (see Fig. 1 and Table S1) by considering the 'dark state' to be an admixture of S_1Q_A-Fe^{2+} and S_1Q_A-Fe^{3+}. Corresponding EPR measurements in apo-WOC confirmed that the apo-WOC/ reassembled sample had approximately the same fraction of centers with an oxidized non-heme iron (up to ~50%). These values provide upper estimates for the fraction of centers that could potentially 'double turnover' – progress through two S-state transitions upon a single 60 μs flash – in the two samples. These are consistent with the parameters given in Table S1. EPR conditions: microwave frequency, 9.27 GHz; microwave power, 12.7 mW; modulation amplitude, 20 G; temperature, 5 K.

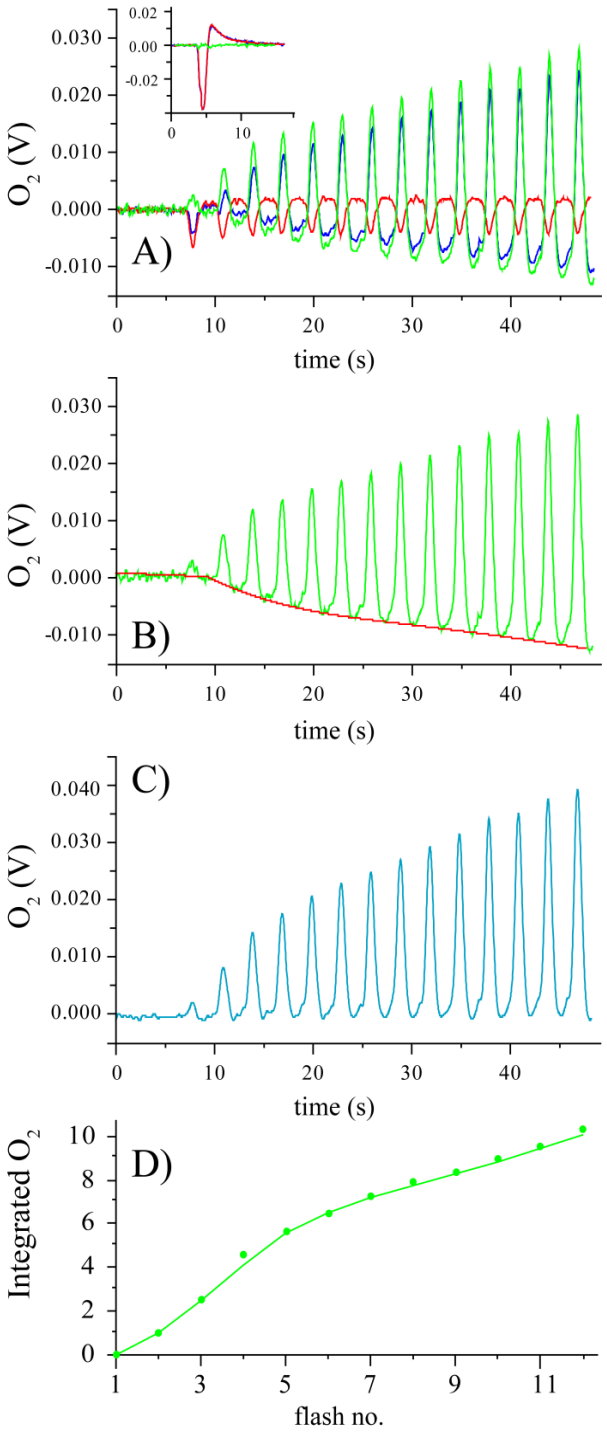

Fig. S5 shows all of the corrections that were made to the raw O_2 data. Tiles A through D show traces representing flashes 2 through 14 of respective experiments, while the inset in Tile A shows flash 1 of the experiments. Two corrections were required: 1) a baseline was subtracted from the data to remove a constant flash artifact; Tile A shows the raw data (blue trace), the baseline (red trace), and the difference or baseline-removed data (green trace). The baseline was generated by repeating the photo-assembly experiment using an apo-WOC sample in which

exogenous Mn was not added. Subtraction of this baseline served the additional purpose of eliminating the background O_2 signal that apo-WOC samples can exhibit arising from a small fraction of centers that were not extracted prior to the experiment (<2% of centers). 2) A second broad spline offset also needed to be subtracted from the flash artifact corrected data; Tile B shows the baseline-removed data (green trace) that was fitted by the spline (red trace) and Tile C shows the difference between the two (e.g., the corrected data). This baseline decrease that is removed by the spline appears due to the use of a notch filter which removes signals outside of 0.3 to 3 Hz frequency range. This filter effectively takes the derivative of the raw amplitude. The signal is then cut on the negative side of the derivative corresponding to its slowest responding component. Tile D shows the integrated O_2 per flash determined from the corrected data seen in Tile C.

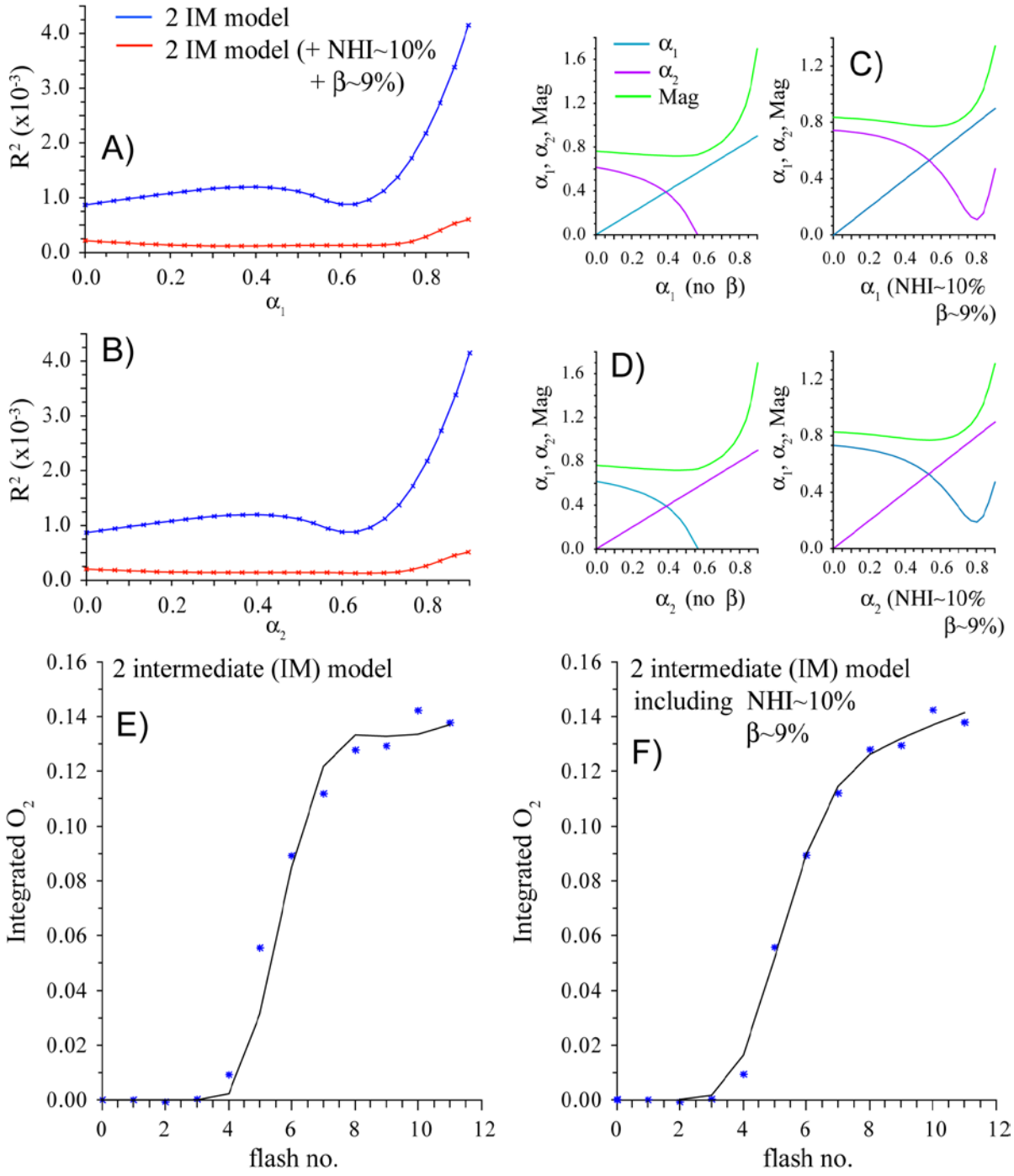

Figure S6: Analysis of photo-assembly model 2 IM. Tiles A and B: one co-ordinate residue (R^2) landscape of the Kok parameters assuming either i) no double hits during photoactivation (red traces), ii) 10% pre-oxidized non-heme iron (NHI). Tiles C and D: corresponding behavior of the other free variables for all values of α_1 (Tile C) and α_2 (Tile D). Tiles E and F: Best fit of integrated photo-assembly curve for the O_2 recovery of apo-WOC assuming either i) no double hits during photoactivation (red traces), ii) 10% pre-oxidized NHI. Kok parameters used for the S-state cycle were determined independently, see Fig. S3. Photo-assembly steps are described by the miss parameter (α_X, note γ_X= 1-(α_X+β). S-state transitions used the parameter set

extracted from fitting the O_2 oscillation pattern observed in reassembled PS II (see "*O_2 oscillations in reassembled PS II membranes*" and Fig. 2).
Fitting of the O_2 response curve could also be improved by assuming a 'non-heme-iron effect', see Figs. S1 and S3. As the dark time between the first and second flash is long (~240 s), it is expected that the non-heme iron will partial re-oxidize during this time, (see above section *O_2 oscillation patterns in reassembled systems).* Two dark non-heme-iron levels were tried: 10% and 20% i.e. approximately the upper and lower limits observed for all PS II samples.

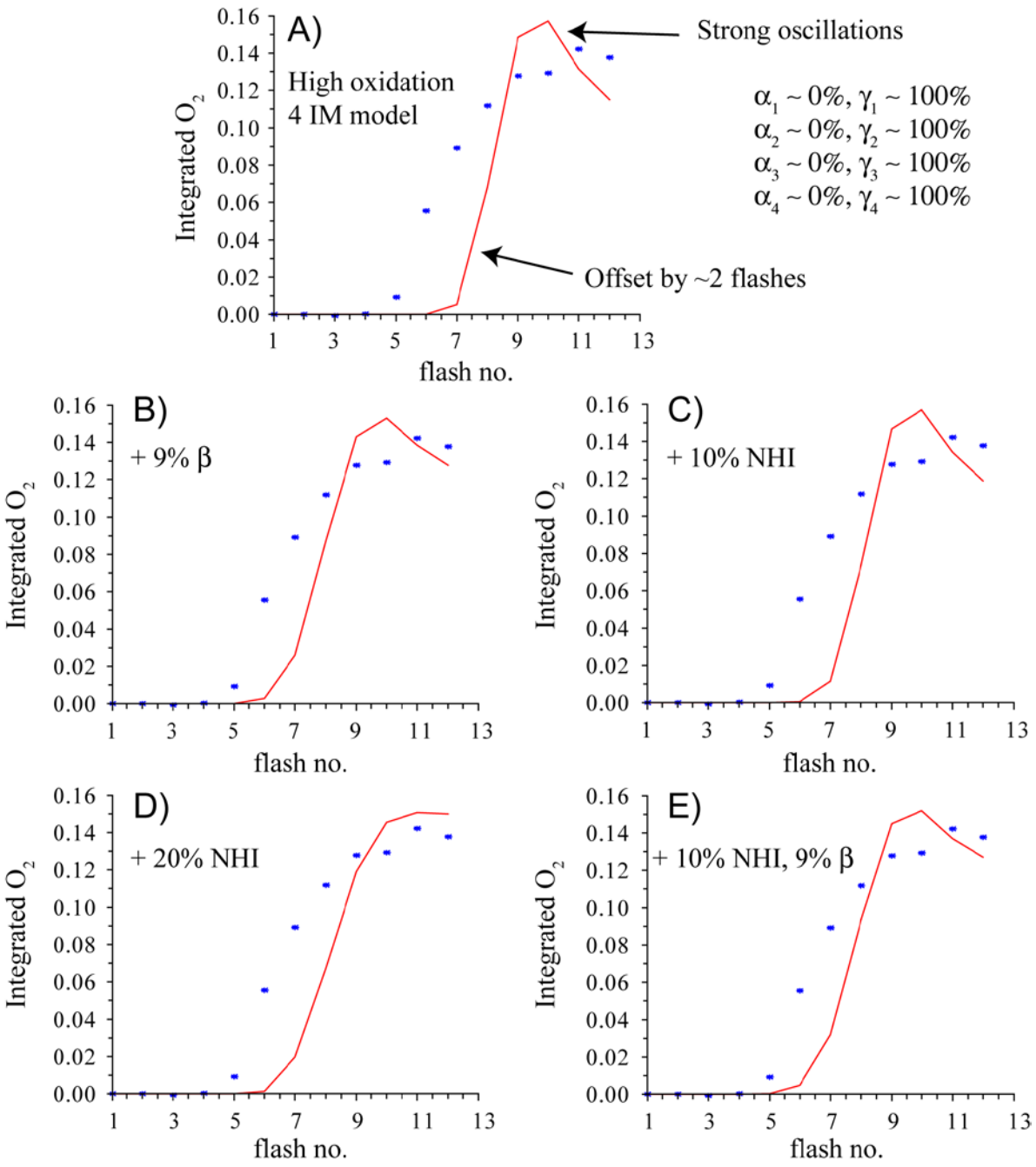
A)
High oxidation
4 IM model
Strong oscillations
$\alpha_1 \sim 0\%, \gamma_1 \sim 100\%$
$\alpha_2 \sim 0\%, \gamma_2 \sim 100\%$
$\alpha_3 \sim 0\%, \gamma_3 \sim 100\%$
$\alpha_4 \sim 0\%, \gamma_4 \sim 100\%$
Offset by ~2 flashes
Integrated O_2
flash no.
B)
+ 9% β
C)
+ 10% NHI
D)
+ 20% NHI
E)
+ 10% NHI, 9% β

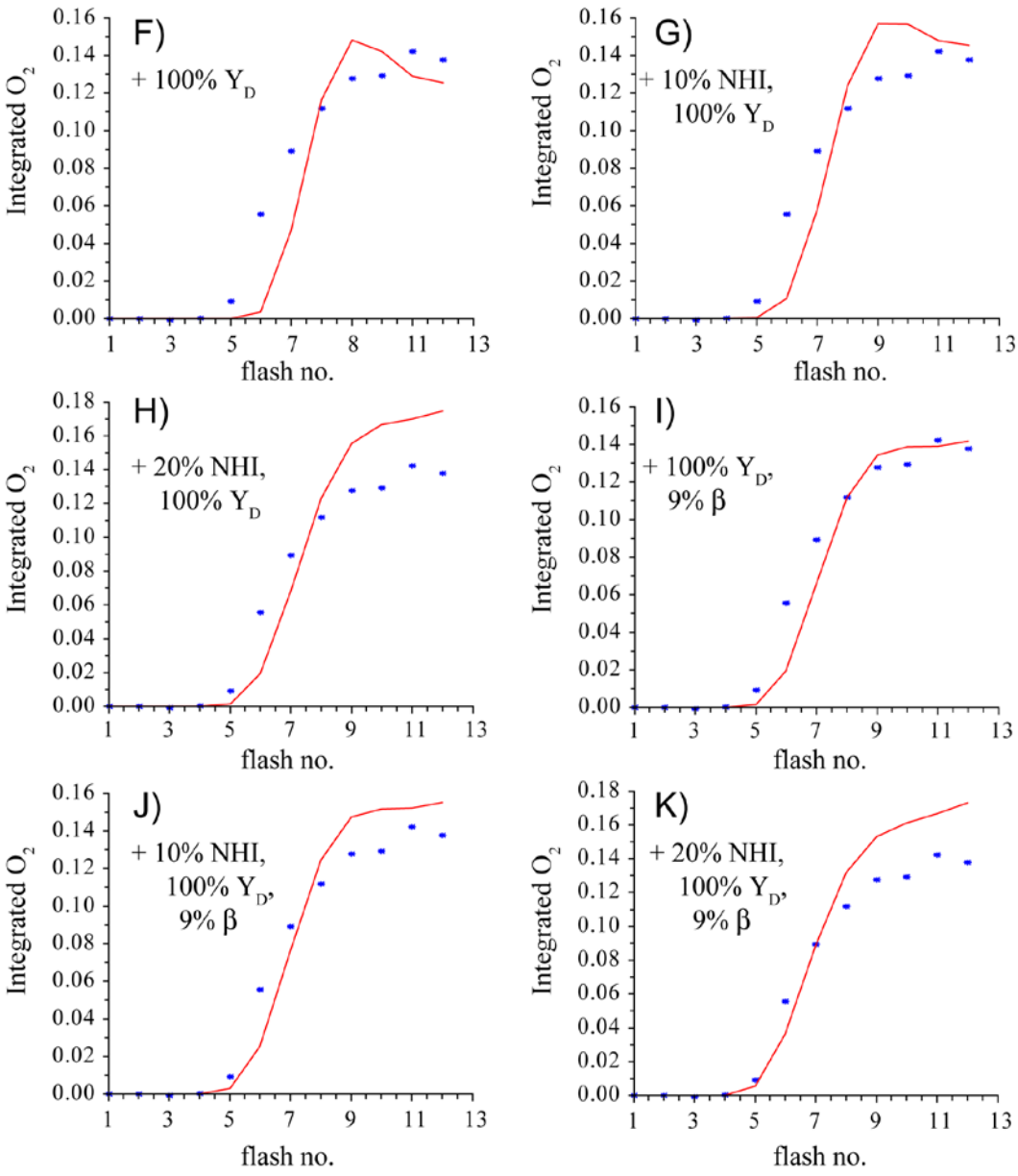

Figure S7: Analysis of photo-assembly model 4 IM. Tile A: Best fit of integrated photo-assembly curve for the O_2 recovery of apo-WOC assuming the majority of centers are initially in the IM_1^* state prior after the 'first flash' (as defined in the text, see Results and Discussion). Tile B: same as Tile A and assumes 9% double hits for all photo-assembly steps. Tile C: same as Tile A and assumes 10% pre-oxidized NHI. Tile D: same as Tile A and assumes 20% pre-oxidized NHI. Tile E: same as Tile A and assumes 9% double hits for all photo-assembly steps and 10% pre-oxidized NHI. Tile F: same as Tile A and assumes one Mn oxidation event occurs in the dark via Y_D. Tile G: same as Tile A and assumes one Mn oxidation event occurs in the dark via Y_D and 10% pre-oxidized NHI. Tile H: same as Tile A and assumes one Mn oxidation event occurs in the dark via Y_D and 20% pre-oxidized NHI. Tile I: same as Tile A and assumes one Mn oxidation event occurs in the dark via YD and 9% double hits for all photo-assembly steps. Tile J: same as Tile A and assumes one Mn oxidation event occurs in the dark via Y_D, 9% double

hits for all photo-assembly steps and 10% pre-oxidized NHI. Tile K: same as Tile A and assumes one Mn oxidation event occurs in the dark via Y_D, 9% double hits for all photo-assembly steps and 20% pre-oxidized NHI.

Modeling photo-assembly (4-intermediate model)

The analogous 4 IM is discussed here. Its basic structure is identical to the 2 IM. Namely the early phase of photo-activation, IM_0 to IM_1 was not included; the model starts at the IM_1^* to IM_2 transition (see Fig. 7). As above, photo-assembly steps are described by the parameters: hit (γ_i), miss (α_i) and double hit (β). α_i and, as a consequence, γ_i, were allowed to vary for each photoactivation step, whereas the β parameter was fixed. S-state transitions used the parameter set (α, γ, β, ε) extracted from fitting the O_2 oscillation pattern observed in reassembled systems (see "*O_2 oscillations in reassembled PS II membranes*"). All centers were assumed to start in the IM_1^* state. Initially, $\beta = 0\%$ was assumed for all photo-assembly steps. Simulations using this assumption are shown in respective tiles. Broadly, this model cannot explain the observed 6th flash O_2 response seen upon photo-assembly of apo-WOC. The simulated photo-assembly curve is offset by 2 flashes and resolves strong oscillations not observed in the data. Fitting of the O_2 response curve was not dramatically improved by including a $\beta = 9\%$ for each photo-assembly step, the inclusion of the 'non-heme-iron effect' (as above for the 2 intermediate model), or a combination of both.
It has been proposed in the literature that Y_D may play a role in WOC assembly. This effect was also allowed for by assuming that Y_D oxidized 1 Mn during the dark step (~240 s). This correction on its own, however, does not dramatically improve the 4 IM simulation. However, with both a Y_D oxidation and 9% double hit and/or non-heme-iron effect, the 4 IM begins to resolve the observed 6 flash O_2 response. It is noted though, these fitting are significantly poorer (larger residuals) than the corresponding fittings for the 2 IM. They also require near unity Mn oxidation events for multiple photo-assembly steps, which is improbable.

Biological repeats:

1) The photoactivation curves (Fig 7) shown are the average of two separate data sets, collected on two separate days, using two separate PSII samples (same PSII stock, but two separate APO treatments).
2) Data set A included 4 separate trials/repeats.
3) Data set B included 5 separate trials/repeats.
4) The trials from each data set where averaged and then integrated. The reproducibly of the raw data is shown below (data set B). It is important to note that the data points of Fig. 7 represent an integration of the O_2 peak across a user defined integration window, thus enhancing the S/N and suppressing systematic errors due to flash artifact subtraction and baseline drift.
5) (Fig S8) The two integrated data sets are also shown below. The same O_2 response was observed i.e. the initial O_2 response curve is nominally identical, a 100% increase in the O_2 level was observed at flash 6. The two data sets do slightly differ after flash 9. This may be due to a population(s) of centers that show good synchronization, and thus do show a small oscillation. This behavior though is not highly reproducible.

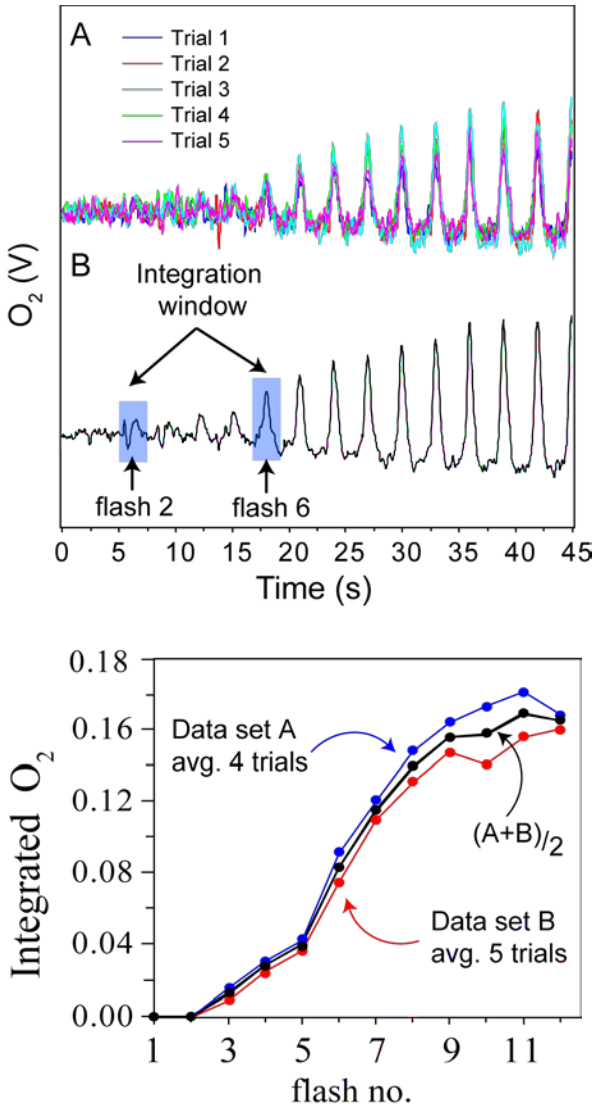

Additional references

56. Buchel, C., J. Barber, G. Ananyev, S. Eshaghi, R. Watt, and C. Dismukes. 1999. Photoassembly of the manganese cluster and oxygen evolution from monomeric and dimeric CP47 reaction center photosystem II complexes. Proc. Natl. Acad. Sci. USA 96:14288-14293.

57. Seidler, A., and A. W. Rutherford. 1996. The role of the extrinsic 33 kDa protein in Ca^{2+} binding in Photosystem II. Biochemistry 35:12104-12110.

58. Baranov, S. V., G. M. Ananyev, V. V. Klimov, and G. C. Dismukes. 2000. Bicarbonate Accelerates Assembly of the Inorganic Core of the Water-Oxidizing Complex in Manganese-Depleted Photosystem II. Biochemistry 39:6060-6065.

59. Diner, B. A., and V. Petrouleas. 1987. Light-Induced Oxidation of the Acceptor-Side Fe(II) of Photosystem-II by Exogenous Quinones Acting through the Qb Binding-Site .2. Blockage by Inhibitors. Biochim. Biophys. Acta 893:138-148.
60. Petrouleas, V., and B. A. Diner. 1987. Light-Induced Oxidation of the Acceptor-Side Fe(II) of Photosystem-II by Exogenous Quinones Acting through the Qb Binding-Site .1. Quinones, Kinetics and Ph-Dependence. Biochim. Biophys. Acta 893:126-137.